Atomic core structure and mobility of [100](010) and [010](100) dislocations in MgSiO₃ perovskite

P. Hirel [*], A. Kraych, P. Carrez, P. Cordier

Unité Matériaux et Transformations, Bât. C6, Universit de Lille 1, 59655 Villeneuve d'Ascq, France

Abstract

The plastic behavior of MgSiO₃ perovskite is investigated under pressure conditions similar to those encountered in the Earth's lower mantle. The core structures of dislocations with edge and screw characters are determined by means of atomic-scale simulations for the [100](010) and [010](100) slip systems. The corresponding Peierls stresses increase monotonously with increasing pressure. The edge [010](100) dislocation is found to dissociate by climb and to become sessile at high pressure ($P \geqslant 80$ GPa). These findings are compared with a continuum Peierls–Nabarro model and with published results in other perovskite materials.
© 2014 Acta Materialia Inc. Published by Elsevier Ltd. This is an open access article under the CC BY-NC-ND license (http://creativecommons.org/licenses/by-nc-nd/3.0/).

Keywords: Computer simulation; Perovskites; Crystal plasticity; Dislocations; Pressure-dependent plasticity

1. Introduction

Geological processes occurring at the surface of the Earth, such as plate tectonics, volcanic activity and seismic activity, are triggered by large-scale convection in the solid state within deeper layers, i.e. in the upper and lower mantle. The latter, corresponding to depths from 670 to 2900 km below the surface, represents over 60% of the mass of our planet, and its composition is dominated by the $(Mg, Fe, Al)(Si, Al) O_3$ perovskite [1,2]. Therefore, determining the properties of defects in this phase is critical for understanding the convection in, and the rheology of, the Earth's interior, but is very challenging due to the extreme conditions that apply at these depths: pressures ranging from 30 to 140 GPa, temperatures from 500 to 2500 °C, and strain rates from 10^{-12} to 10^{-16} s^{-1}.

The microstructure of the perovskite phase is expected to be polycrystalline with grain sizes ranging from 0.01 to several millimeters [3], large enough to allow for intragranular plasticity. Only few experiments have been able to deform magnesium silicate perovskite in conditions relevant to the lower mantle [4,5]. If controlling the pressure and temperature conditions remains highly challenging, the relevant deformation rates—equivalent to thousand-year experiments—are simply impossible to achieve in the laboratory. However, numerical simulations can be utilized to shed light on the behavior of phases under these very peculiar conditions [6].

In this work we investigate the plastic behavior of the Mg-rich end-member of this phase, the distorted orthorhombic magnesium silicate MgSiO₃ perovskite (hereinafter referred to as Mg-Pv). The choice of slip systems investigated in the present study is driven by the analogy with cubic and tetragonal perovskites, where the reported easiest slip systems are systematically $\langle 110 \rangle \{1\bar{1}0\}$ in cubic SrTiO₃ [7–10], tetragonal BaTiO₃ [7,11], CaGeO₃ [12], CaTiO₃ [13,14], and CaSiO₃ [15,16]. Because of its distorted orthorhombic structure the equivalent slip systems are [100](010) and [010](100) in Mg-Pv, i.e. the slip systems with the lowest indexes (see e.g. Fig. 1 in Ref. [5]). Moreover dislocations with Burgers vectors [100] and

* Corresponding author.
    E-mail address: pierre.hirel@univ-lille1.fr (P. Hirel).

[0 1 0] were observed experimentally [5], and previous calculations using a Peierls–Nabarro model suggest that these two slip systems are the easiest ones [17].

The intrinsic properties of dislocations are determined for these two slip systems by means of atomic-scale simulations, in the range of pressures 30–140 GPa relevant to the Earth's lower mantle. The atomic core structure, the Peierls stress and their dependence on the isostatic pressure are investigated.

2. Methods and models

Mg-Pv is a high-pressure phase, stable only in the pressure range $P = 26$–130 GPa [18–20], and crystallizes in a distorted orthorhombic lattice [21,22]. In this work we describe it with the *Pbnm* space group, where [1 0 0] is the shortest unit cell vector, [0 1 0] is the second shortest and [0 0 1] is the longest. The occupied Wyckoff positions are (4*c*) for Mg ions, (4*b*) for Si ions, and (4*c*) and (8*d*) for O ions. The lattice parameters depend on pressure, and range from $a_0 = 4.6481$ Å, $b_0 = 4.7615$ Å, $c_0 = 6.7178$ Å at $P = 30$ GPa, to $a_0 = 4.3379$ Å, $b_0 = 4.4923$ Å, $c_0 = 6.2805$ Å at $P = 140$ GPa with the interatomic potential described below (the subscript 0 means that the lattice parameters are the ones optimized at 0 K).

Classical atomistic simulations are performed with the LAMMPS package [23]. The potential energy between two ions of different indices i and j is described by a rigid-ion pair potential function:

$$U_{ij} = \frac{q_i q_j}{R_{ij}} + b_{ij} \exp\left(\frac{-R_{ij}}{\rho_{ij}}\right) - \frac{c_{ij}}{R_{ij}^6} \tag{1}$$

where q_i and q_j are the electric charges of ions i and j, R_{ij} the distance between them, and b_{ij}, ρ_{ij} and c_{ij} adjustable parameters. We use the parametrization by Oganov and coworkers [24], reported in Table 1. This potential was fitted to reproduce the lattice parameters, elastic constants, thermal expansion coefficient and phonon density of states in the pressure range 30–140 GPa. More recently it was used to compute generalized stacking fault (GSF) energy densities, and was shown to reproduce ab initio results with good accuracy [25], which justifies its use to model dislocations [26].

The atomic systems are designed to study the motion of a single dislocation, as illustrated in Fig. 1. The dislocation line lies along the Cartesian z direction, the glide plane is normal to the y direction, and the direction of glide is aligned with the x axis. The crystallographic directions
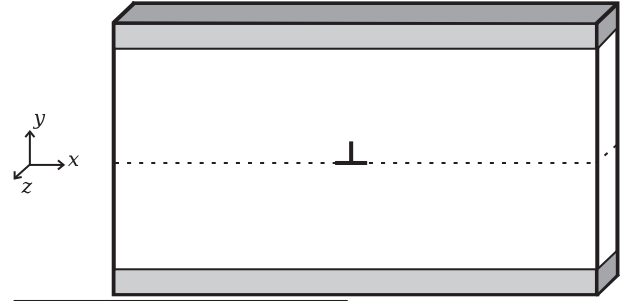
Dislocation	x	y	z
[100](010) screw	[001]	[010]	[100]
[100](010) edge	[100]	[010]	[001]
[010](100) screw	[001]	[100]	[010]
[010](100) edge	[010]	[100]	[001]

Fig. 1. Geometry of the systems used in atomistic simulations. The slip plane is symbolized with a dashed line, and the top and bottom shaded areas are zones where atoms are kept fixed. The actual crystal orientations used to model each type of dislocation are reported in the table.

depend on the slip system studied (see table in Fig. 1). A periodic cluster approach is used, where the system is periodic along x and z, and the atoms located at the top and bottom of the supercell along the y axis are maintained fixed to mimic an infinite perfect crystal and avoid spurious elastic interaction between periodic replicas. The simulation supercells are as thin as a single unit cell vector along the z direction, so as to simulate a straight, infinite dislocation line. For screw dislocations the supercell has a depth equal to the Burgers vector b along the dislocation line, and the first supercell vector is given a component $b/2$ along z so that the boundaries of periodic replicas match along x. Edge dislocations are constructed by the superposition of two supercells, the top one containing an extra atomic plane. The relaxation of such a system yields an edge dislocation [27]. For the sake of charge neutrality, all dislocations are constructed so that stoichiometry is preserved.

In such a simulation setup the dislocation interacts with its periodic replicas along the x axis; however, the dislocation is by definition always equidistant to the two replicas surrounding it, so the contributions of these two replicas cancel each other. Moreover the size of the supercells was increased until the results were converged. Typical supercells have a size about $180 \times 170 \times 6$ Å and contain about 30,000 ions.

Molecular statics simulations are performed at constant volume, and the positions of atoms are optimized using a conjugate-gradient algorithm until the maximum force on an atom drops below 10^{-11} eV Å^{-1} (1.602×10^{-20} N).

Dislocations are characterized by computing the atomic disregistry $\phi(x)$ for each cation sublattice (Mg and Si). The derivative of the disregistry $d\phi(x)/dx$ corresponds to the density of Burgers vector in the glide plane, and its full width at half maximum is used to define the width of the dislocation core [28]. The oxygen sublattice has a different density and its disregistry is not computed.

Table 1
Parameters used in the interatomic potential (Eq. (1)). Electric charges q_i are in units of the elementary charge e, the b_{ij} in eV, the ρ_{ij} in Å, and the c_{ij} in eV Å^{-6}. After Oganov et al. [24].

$i - j$	q_i	b_{ij}	ρ_{ij}	c_{ij}
Mg–O	1.9104	1041.435	0.2866	0.00
Si–O	2.9043	1137.028	0.2827	0.00
O–O	−1.6049	2023.800	0.2674	13.83

In deformation simulations, an appropriate simple shear strain is applied to maximize the shear stress in the glide plane (ϵ_{yx} and ϵ_{yz} for edge and screw dislocations, respectively) by increments of 0.1%, the force minimization procedure being applied at each increment. The corresponding stress is determined from the derivative of the system's potential energy with respect to the shear displacements. Monitoring the derivative of the disregistry allows precise determination of the stress required to move the dislocation in the absence of temperature, i.e. the Peierls stress.

Isostatic pressure is introduced by scaling the supercell in each direction by the appropriate factor to reach the target pressure, according to the equation of state [24]. After that the supercell dimensions are fixed and only the positions of ions are optimized to determine the dislocation core structure and the Peierls stress.

3. Results

In this section we detail the core structure, Peierls stress and the influence of pressure for each type of dislocation.

3.1. The [100](010) screw dislocation

We begin with a description at the isostatic pressure $P = 30$ GPa of the screw dislocation with a [100] Burgers vector. The atomic displacement map at the top of Fig. 2 shows that this dislocation is planar and spreads into the (010) plane. The atomic disregistry ϕ in that plane, and its derivative $d\phi/dx$, are reported in Fig. 2 for the cationic sublattices. It shows that the dislocation has a compact, symmetric core structure, with a width $\zeta = 9.4$ Å.

As illustrated in Fig. 3, the dislocation core contains one pair (per Burgers vector) of SiO_6 octahedra that are connected by their edges, instead of their corners as in the bulk. This configuration resembles that of an anti-phase boundary (APB), a type of stacking fault observed in other perovskites [29] and also observed in the core of dislocations in other perovskites [30,31].

When the applied isostatic pressure is increased from 30 to 140 GPa, the atomic structure of the dislocation remains identical. The width of the dislocation core scales linearly with the lattice parameter: $\zeta = 1.5c_0$.

Next we model the motion of the [100] screw dislocations in the (010) plane by applying a shear strain ϵ_{yz} in increments of 0.1%. Monitoring the stress and the derivative of the disregistry allows us to determine the critical stress at which the dislocation moves, i.e. the Peierls stress, for different applied pressures. The Peierls stress increases linearly from $\sigma_P = 5$ GPa at $P = 30$ GPa, to $\sigma_P = 15$ GPa at $P = 140$ GPa, as marked by the empty circles in Fig. 9.

3.2. The [100](010) edge dislocation

Similarly we investigated the atomic structure of the [100](010) edge dislocation, which is reported at the top of Fig. 4. Inside the dislocation core two rows of SiO_6
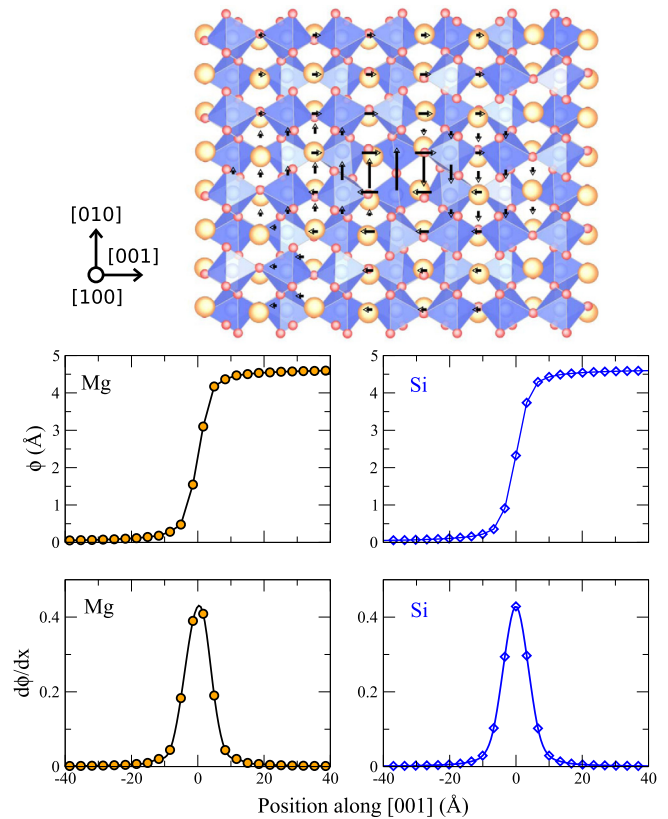

Fig. 2. Top: atomic configuration of the screw dislocation with a [100] Burgers vector at $P = 30$ GPa, viewed along the dislocation line. Mg ions are represented by large orange spheres, Si ions by medium blue spheres, and O ions by small red spheres. SiO_6 octahedra are shown in transparent blue. Arrows represent the relative displacement along the [100] direction between two ions. Bottom: corresponding disregistry $\phi(x)$ and Burgers vector density $d\phi/dx$ for the Mg (spheres) and Si (diamonds) sublattices. (For interpretation of the references to colour in this figure caption, the reader is referred to the web version of this article.)
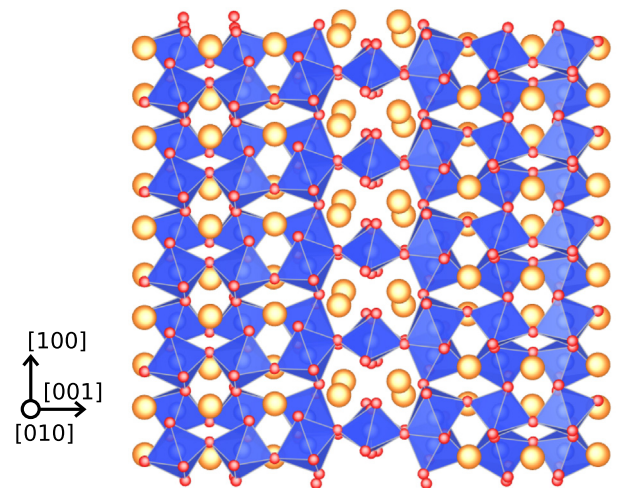
Fig. 3. Atomic configuration of the [100] screw dislocation viewed in the (010) plane.

octahedra are connected by their edges, which is again similar to an APB. Although in the cell the stoichiometry is preserved, inside the dislocation core some octahedra have

Fig. 4. Top: atomic configuration of the $[100](010)$ edge dislocation at $P = 30$ GPa, viewed along the dislocation line (same color conventions as in Fig. 2)). Bottom: corresponding disregistry $\phi(x)$ and Burgers vector density $d\phi/dx$ for the Mg (spheres) and Si (diamonds) sublattices. (For interpretation of the references to colour in this figure caption, the reader is referred to the web version of this article.)
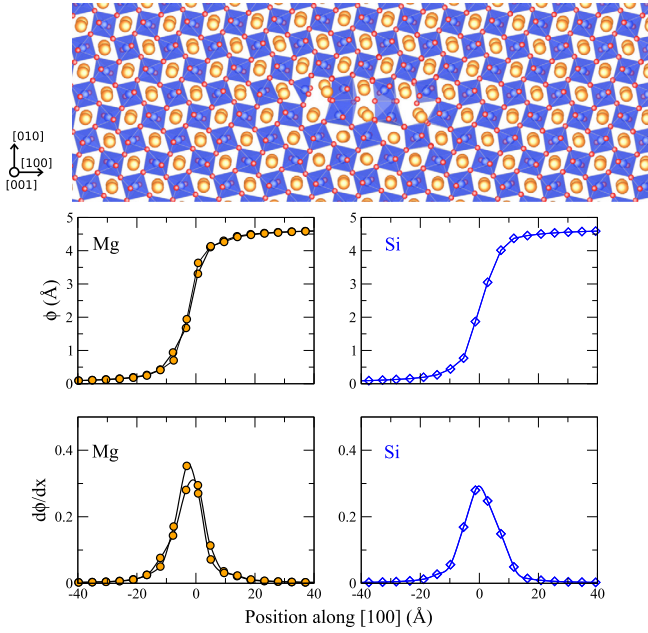
an incomplete SiO$_5$ coordination. The atomic structure of the dislocation core is clearly asymmetric along the $[100]$ axis. Also, the period along the dislocation line is $[001]$, i.e. the picture actually shows two $1/2[001]$ planes superimposed along the viewing direction. One can see that the atom positions are slightly different in those two planes.

These features appear more clearly when analyzing the disregistry $\phi(x)$, reported on the graphs in Fig. 4. The disregistry of the Mg sublattice confirms that the atomic displacements differ in the two adjacent (001) planes normal to the dislocation line, while the disregistry for the Si sublattice is the same in those two planes. The derivative of the disregistry $d\phi/dx$ shows that the dislocation is non-symmetric, and its width is estimated to $\zeta = 13$ Å at $P = 30$ GPa. This is almost perfectly a factor $(1 - v)$ broader than the $[100](010)$ screw dislocation, as predicted by the elastic theory of dislocations (with $v = 0.34$ as determined with the atomistic potential).

When increasing pressure up to 140 GPa the atomic structure of this dislocation does not change. The width of the dislocation core scales almost perfectly with the lattice parameter: $\zeta = 2.8a_0$.

We studied the motion of the $[100](010)$ edge dislocation by applying a simple shear strain ϵ_{yx}. The Peierls stress is different when applying a positive or a negative shear, e.g. at 30 GPa the Peierls stress is $\sigma_P^- = 4.79$ GPa to move the dislocation in the $[\bar{1}00]$ direction ($\epsilon_{yx} < 0$), and $\sigma_P^+ = 5.19$ GPa to move it in the $[100]$ direction ($\epsilon_{yx} > 0$). This behavior is obviously related to the fact that the dislocation core is non-symmetric.
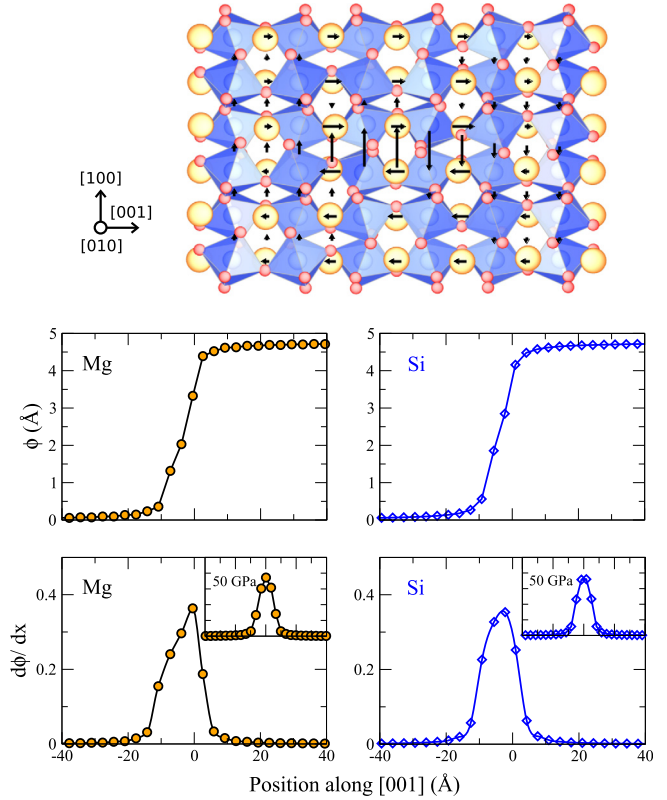

Fig. 5. Top: atomic configuration of the screw dislocation with a $[010]$ Burgers vector at $P = 30$ GPa, viewed along the dislocation line (same color conventions as in Fig. 2). Arrows represent the relative displacement along the $[010]$ direction between two ions. Bottom: corresponding disregistry $\phi(x)$ and Burgers vector density $d\phi/dx$ for the Mg (spheres) and Si (diamonds) sublattices. The inset graphs show the Burgers vector density for the Mg and Si sublattices at $P = 50$ GPa. (For interpretation of the references to colour in this figure caption, the reader is referred to the web version of this article.)

Because of the particular symmetry of the lattice, the situation is expected to be reversed if the dislocation glides in another (010) glide plane at a different height, shifted by $1/2[010]$. We constructed such a system, and when applying shear strain we obtained that it is easier to glide along $[100]$ than along $[\bar{1}00]$, i.e. the inverse of before. For the sake of clarity we report only the values of the Peierls stress that correspond to the easiest direction of glide in Fig. 9 (filled circles).

When the pressure is increased up to 140 GPa the Peierls stress increases linearly, from 4.79 GPa at 30 GPa to 7.11 GPa at 140 GPa, as reported on Fig. 9 (filled circles).

3.3. The $[010](100)$ screw dislocation

We now discuss the core structure of the $[010]$ screw dislocation. This dislocation is expected to be very similar to the $[100]$ screw dislocation because the magnitudes of their Burgers vectors, respectively b_0 and a_0, are very close to one another, and so are the spacings between the glide planes.

The displacement map at the top of Fig. 5 shows that the core of this dislocation is also planar and spreads in
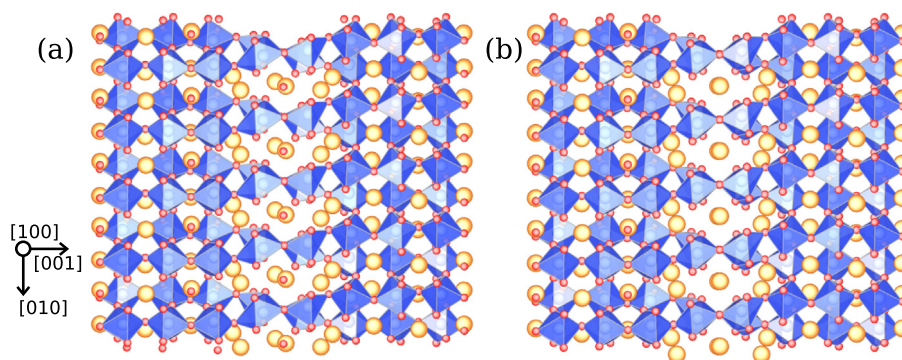
Fig. 6. Atomic configuration of the [010] screw dislocation viewed in the (100) plane (same color conventions as in Fig. 2) at the isostatic pressures: (a) $P = 30$ GPa; (b) $P = 50$ GPa. (For interpretation of the references to colour in this figure caption, the reader is referred to the web version of this article.)
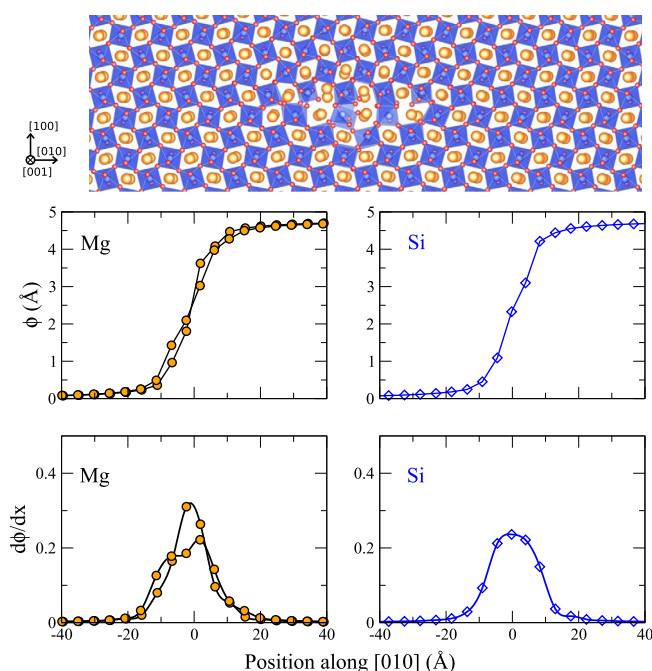

Fig. 7. Top: atomic configuration of the [010](100) edge dislocation at 30 GPa, viewed along the dislocation line (same color conventions as in Fig. 2). Bottom: corresponding disregistry $\phi(x)$ and Burgers vector density $d\phi/dx$ for the Mg (spheres) and Si (diamonds) sublattices. (For interpretation of the references to colour in this figure caption, the reader is referred to the web version of this article.)

the (100) plane. The analysis of the disregistry (Fig. 5) confirms spreading in the (100) plane. The atomic structure of the core is strongly distorted and non-symmetric. The width of the dislocation core is estimated to $\zeta = 12.5$ Å $= 1.86c_0$, which is 33% broader than the [100] screw dislocation.

The atomic configuration of the [010] screw dislocation in its spreading plane (100) is represented in Fig. 5 for an isostatic pressure of 30 GPa. The dislocation core contains two pairs (per Burgers vector) of SiO_6 octahedra connected by their edges (Fig. 6a), which is consistent with the fact that this dislocation has a broader core than the [100]

dislocation. In addition, one of these octahedra has an incomplete SiO_5 coordination.

At pressures greater than 50 GPa the core structure becomes markedly different: all the Si ions have an ideal SiO_6 coordination as in the bulk (Fig. 6b), and the Burgers vector density becomes highly symmetric, as shown in the inset graphs in Fig. 5. The core becomes more compact, with a width $\zeta = 11.78$ Å. The [010] screw dislocation is characterized by this symmetric core structure for pressures up to 140 GPa, and the core width scales with the lattice parameter: $\zeta = 1.78c_0$, i.e. 19% broader than the [100] screw dislocation.

The motion of the [010] screw dislocation was simulated in the (100) plane. In the pressure range 30–50 GPa we find that the Peierls stress is different when applying a positive or negative shear, e.g. at 30 GPa the Peierls stress is $\sigma_P^+ = 11.45$ GPa to move the dislocation in the [001] direction ($\epsilon_{yz} > 0$), and $\sigma_P^- = 4.52$ GPa to move it in the [00$\bar{1}$] direction ($\epsilon_{yz} < 0$). This effect is similar to that observed for the [100](010) edge dislocation, and is due to the non-symmetric core structure of the [010] screw dislocation in this pressure range. Again only the lowest values of the Peierls stress are considered in the discussion below. At pressures higher than 50 GPa the dislocation core structure becomes symmetric, and the Peierls stress is the same for positive and negative applied strain. It increases monotonously up to $\sigma_P = 15$ GPa at $P = 140$ GPa, as indicated by the empty squares in Fig. 9.

3.4. The [010](100) edge dislocation

Finally we investigate the properties of the [010](100) edge dislocation, the atomic structure of which at 30 GPa is reported in Fig. 7. Features similar to the [100](010) edge dislocation can be observed, i.e. two pairs of SiO_6 octahedra connected by their edges and incomplete SiO_5 coordination inside the core. The computation of the disregistry shows that this dislocation is also strongly non-symmetric, with a width $\zeta = 17.5$ Å. Again this width is greater than the width of the [010] screw dislocation by a factor $(1 - \nu)$, as predicted by the elastic theory of dislocations. In addition

the displacement of Mg ions is markedly different in the two adjacent (001) layers normal to the dislocation line.

When applying shear strain, we found again that the behavior of the [010](100) edge dislocation depends on the sign of the applied shear strain, e.g. at 30 GPa we found $\sigma_P = 4.75$ GPa for $\epsilon_{yx} > 0$ and $\sigma_P = 2.70$ GPa for $\epsilon_{yx} < 0$. As explained previously, only the lowest values are reported in Fig. 9 (filled squares).

At low pressures up to 70 GPa the atomic structure of the [010](100) edge dislocation remains identical to that at 30 GPa, and the Peierls stress increases up to 9 GPa at 70 GPa. The width of the dislocation scales linearly with the lattice parameter: $\zeta = 3.67 b_0$.

Between 70 and 80 GPa this atomic configuration becomes unstable, and the dislocation adopts a markedly different core structure: the two SiO_6 octahedra sharing an edge form a stacking fault in the (010) plane (instead of the (100) glide plane), as illustrated in Fig. 8. This dislocation core is non-planar, and can be described as two partial dislocations of Burgers vectors 1/2[010] dissociated by climb in the (010) plane. We note that this stacking fault is the same as the one that exists in the core of the glide-spread [100](010) edge dislocation described before. Because of this peculiar core structure the [010] edge dislocation becomes sessile: no glide could be observed at any level of applied strain, and hence no Peierls stress can be reported above 70 GPa in Fig. 9.

4. Discussion

4.1. Differences between dislocations [100] and [010]

As mentioned in the Introduction, based on the equivalence between the perfect cubic and the distorted orthorhombic perovskite structures, dislocations in Mg-Pv with [100] and [010] Burgers vectors were a priori expected to be very similar. These two crystallographic directions can indeed be viewed as ⟨110⟩ pseudo-cubic directions with comparable lattice parameter a_0 and b_0, which do not differ by more than 5% over the whole pressure range investigated here (e.g. $a_0 = 4.6481$ Å and $b_0 = 4.7615$ Å at 30 GPa). Surprisingly we find that the properties of these
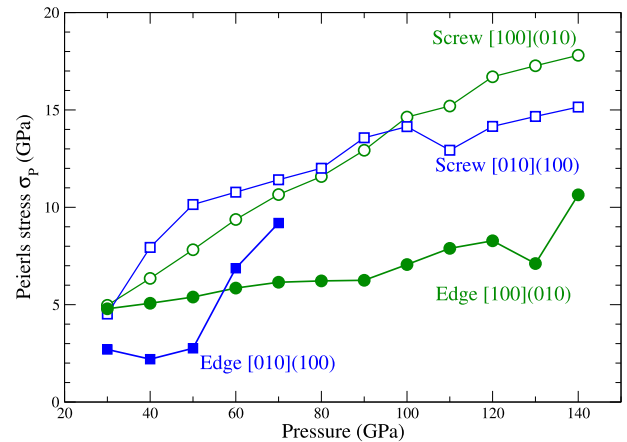

Fig. 9. Dependence on the isostatic pressure of the Peierls stress for the various dislocations studied: [100](010) screw (open circles), [010](100) screw (open squares), [100](010) edge (filled circles), [010](100) edge (filled squares). The latter becomes sessile above 80 GPa.

dislocations differ considerably. The core of the [010] screw dislocation is 33% broader than that of the screw [100], and the same holds between dislocations with edge character. These differences cannot be explained by elastic effects, since the shear moduli for [100] and [010] dislocations in Mg-Pv do not differ more than a few per cent [25].

The underlying reason for such large differences in the core structures of [100] and [010] dislocations may come from the high level of distortion associated with the orthorhombic structure. The SiO_6 octahedra are tilted by an angle $\theta_a = 6.9°$ around the [100] axis, and $\theta_b = 16.3°$ around the [010] axis at 30 GPa (both values increase slightly with pressure, but not significantly). Whereas the tilt of SiO_6 octahedra has little effect on the lattice parameters, the difference between θ_a and θ_b results in distinct atomic arrangements inside the dislocation cores. The low tilt value of θ_a allows for symmetric core structures with fully preserved SiO_6 coordination (for [100] screw dislocation). However, the larger value of θ_b seems to lead to a non-symmetric core structure, and to a loss of coordination of octahedra (for [010] screw dislocation at low pressure). In the case of the [010] edge dislocation this large tilt may
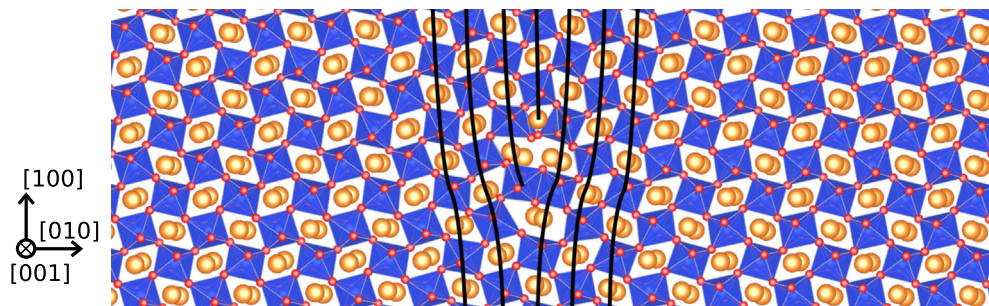

Fig. 8. Most stable configuration of the [010] edge dislocation at $P = 80$ GPa, viewed along the dislocation line (same color conventions as in Fig. 2). Some (010) atomic planes are overlined to evidence the positions of two partial dislocations. (For interpretation of the references to colour in this figure caption, the reader is referred to the web version of this article.)

also be the reason why climb dissociation is more favorable at high pressure.

The modifications in the core structures also have an effect on the mobility of dislocations. The elastic theory of dislocations predicts that wider dislocation cores are often associated with lower values of the Peierls stress [32], and our results are in qualitative agreement with this statement. However, we point out that the Peierls stress can depend on the sign of the applied shear. This behavior always happens when the core structure is not symmetric, i.e. for the edge [100] and [010] dislocations, and for the screw [010] dislocation at low pressure. At pressures greater than 50 GPa the latter adopts a symmetric core structure, and the asymmetry in the Peierls stress vanishes.

Again, the tilt of octahedra in the direction of the glide is probably the underlying factor. For instance, the edge dislocations glide along [100] or [010], i.e. along directions where the tilt of the octahedra breaks the symmetry of the Peierls potential. On the contrary screw dislocations glide along the [001] direction, where the tilt of the octahedra is small and therefore the Peierls potential must be more symmetric.

4.2. Effect of pressure and loss of a slip system

The Peierls stress of the studied dislocations strongly depends on the isostatic pressure, as reported in Fig. 9. While the values are comparable at $P = 30$ GPa, the [010](100) screw dislocation has the highest increasing rate of the Peierls stress up to 50 GPa, probably because of its non-symmetric core structure in this pressure range. The [100](010) screw dislocation has a Peierls stress that increases linearly with increasing pressure, and becomes slightly less mobile than the [010](100) screw dislocation for $P > 100$ GPa. The mobility of the [100](010) edge dislocation is the less dependent on pressure, as it increases linearly from 5 to about 10 GPa over the entire pressure range.

The [010](100) edge dislocation, while being the most mobile at low pressure (30–50 GPa), has a Peierls stress that suddenly increases at 60 GPa. At $P = 80$ GPa the dislocation switches to a climb-dissociated core structure because the two partial dislocations become separated by a stacking fault in the (010) plane. Due to this change in the core structure this dislocation becomes sessile, and no glide could be triggered under applied shear strain. This behavior is unique among the dislocations that we have studied, and suggests that this slip system cannot be activated at pressures above 80 GPa. These dislocations, if they exist, may be able to move only thanks to a climb mechanism.

In order to verify that this behavior is not an artefact of the interatomic potential, we performed simulations employing two other potentials: the one parametrized by Alfredsson et al. [33], and the one proposed by Chen et al. [34]. Both potentials reproduce the behavior obtained with the Oganov potential, i.e. the glide-spread core structure is unstable above 70 GPa and relaxes in a climb-dissociated core structure.

The loss of this slip system at high pressure raises the question of the activation of other slip systems, in particular the glide of [100] and [010] dislocations in the (001) plane. This plane was not considered at first because the [001] direction of the Mg-Pv is equivalent to the cubic [002] direction, therefore it is not a low-index plane of the cubic lattice, nor does it correspond to an easy glide plane in cubic perovskites. However, in the light of the present results it appears that this glide plane needs to be investigated in Mg-Pv. We are currently proceeding with the detailed analysis of these slip systems in order to obtain a more complete picture of dislocation-mediated plastic deformation of Mg-Pv.

4.3. Comparison with continuum model

In a recent study the GSF energy densities (or γ-surfaces) in Mg-Pv have been used to model the core structure and mobility of screw dislocations in the framework of a continuum Peierls–Nabarro–Galerkin (PNG) model [25]. We compare the core widths and values of the Peierls stress obtained in this continuum model with the results obtained with our fully atomistic method.

As an example, the results of the PNG model for the [100] screw dislocation are reported as continuous lines in Fig. 10. The derivative of this continuous disregistry shows two maxima, corresponding to the dissociation of the dislocation with a distance $d = 3.8$ Å between the partials, i.e. smaller than a lattice constant ($c_0 = 6.7178$ Å). This is qualitatively different from our atomistic simulations which predict a compact core (Fig. 2).

The PNG model allows the Burgers vector density to spread continuously so as to minimize the energy of the dislocation core with respect to the GSF energies, without
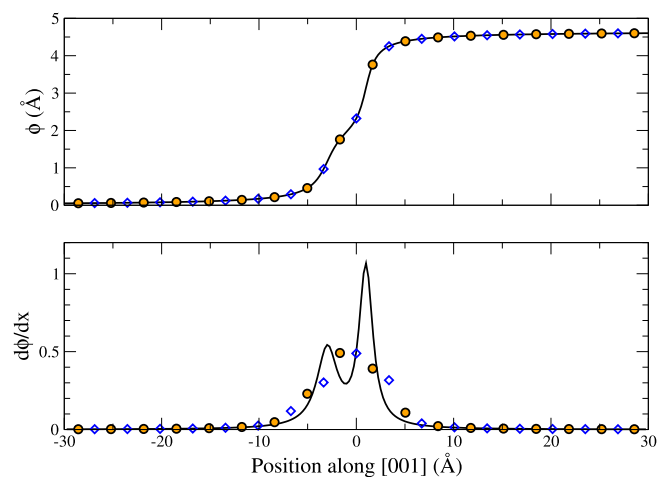

Fig. 10. Top: disregistry ϕ of the [100](010) screw dislocation at 30 GPa determined with the PNG model in Ref. [25] (continuous black lines). The circles and diamonds represent the discretization of the continuous line over the lattice positions of Mg and Si ions, respectively. Bottom: derivative of the continuous PNG disregistry from Ref. [25] (continuous black line), and derivative of the discretized disregistry (circles and diamonds).

accounting for the discreteness of the lattice. The discretization of the disregistry inferred from continuous Peierls–Nabarro models has been argued for in the literature, as it can have an influence on the determination of the Peierls stress especially when the dislocation cores are narrow as in semiconductors [35,36] or in metals [37]. We have discretized the continuous disregistry given by the PNG model over the lattice sites in Mg-Pv (circles and diamonds in Fig. 10). When this discretized disregistry is derived, the Burgers vector density shows only one maximum corresponding to a compact dislocation core. This is in qualitative and quantitative agreement with our atomistic simulations (Fig. 2). This comparison suggests that the continuum disregistry obtained with the PNG model should be interpreted in terms of atomic displacements, and discretized before it is derived to obtain the Burgers vector density. With such a discretization the PNG model leads to a good estimate of the core structures of screw dislocations in Mg-Pv.

It is worth noting that further comparison between continuum and atomistic calculations reveals large discrepancies regarding the evaluation of the Peierls stress. At 30 GPa the Peierls stress required to move the [100](010) screw dislocation is estimated to be 0.2–0.4 GPa in the PNG framework Fig. 2, while our atomistic simulations predict a value of 4.79 GPa. For other slip systems the two methods also differ by a factor of 3–10. Peierls stresses determined with atomistic simulations are systematically higher than ones expected with the continuum model which may be due to the fact that in atomistic simulations atomic interactions are explicitly accounted for, including local effects due to ion charges and electric polarization. When the lattice becomes distorted, as in the core of a dislocation, such effects can become important and play a role in the atomic structure of the defect. Moreover, our atomistic simulations indicate that the [010](100) dislocation becomes non-planar and sessile above 80 GPa. Such a scenario cannot be inferred from the γ-surfaces nor the PNG model, because such frameworks only consider glide in a given plane.

4.4. Comparison with other perovskites

Since experimental deformation of Mg-Pv is difficult because this phase is only stable above 26 GPa, several studies have been performed on analogous materials exhibiting the perovskite structure that are naturally stable under usual laboratory conditions, such as $SrTiO_3$ [38], $BaTiO_3$ [39,40], $CaTiO_3$ [13,39,41], $YAlO_3$ [42], $NaNbO_3$ [41], $KTaO_3$ and $KNbO_3$ [43].

As mentioned in the Introduction, the slip systems [100](010) and [010](100) investigated here in Mg-Pv are equivalent to the slip systems $\langle 110 \rangle \{1\bar{1}0\}$ in cubic perovskites. Despite this equivalence, the intrinsic properties of dislocations in Mg-Pv differ greatly from those of other perovskites. In cubic and tetragonal perovskites the edge and screw dislocations dissociate into two collinear partials with a $1/2\langle 110 \rangle$ Burgers vector separated by an APB, as evidenced by experimental observations [7–9]

and theoretical calculations [10,44]. On the contrary, in the distorted orthorhombic Mg-Pv we find that dislocations with a Burgers vector [100] or [010] have a compact core and do not dissociate. These results are consistent with the γ-surface profiles, which show a double hump and a metastable APB in cubic and tetragonal perovskites [10], whereas no metastable stacking fault is found in Mg-Pv [25].

These results demonstrate that it is hazardous to perform observations or calculations in a prototype perovskite, such as $SrTiO_3$, and extrapolate the results to another perovskite such as Mg-Pv. As was shown in the late 1980s by Beauchesne and Poirier, perovskites do not form an isomechanical group and can have very different plastic behaviors [40,43], as dislocations can have very different properties depending on the lattice distortion, the chemical composition and the thermodynamic conditions.

5. Conclusions

The atomic core structure and mobility of dislocations were investigated for the slip systems [100](010) and [010](100) in $MgSiO_3$ perovskite over the entire pressure range relevant to the Earth's lower mantle. All dislocations are found to have a compact core structure, which is markedly different from cubic or tetragonal perovskite materials where dislocations in the easiest slip systems usually dissociate. The values of the Peierls stress increase monotonously with the applied isostatic pressure. The noticeable exception is the [010](100) edge dislocation, which is found to dissociate by climb and become sessile at pressures greater than 80 GPa.

The study of these two slip systems is a first step in the understanding of the atomic-scale properties of dislocations in Mg-Pv under conditions encountered in the Earth's lower mantle. Other slip systems and other mechanisms, e.g. dislocation climb, need to be considered in order to obtain a more complete understanding of dislocation-mediated plasticity in this material.

Acknowledgements

References

[1] Knittle E, Jeanloz R. Science 1987;235:668–70.
[2] Hemley R, Cohen R. Annu Rev Earth Planet Sci 1992;20:553.
[3] Solomatov V, Reese C. J Geophys Res 2008;113:B07408.
[4] Merkel S, Wenk H, Badro J, Montagnac G, Gillet P, Mao H, et al. Sci Lett 2003;209:351–60.
[5] Cordier P, Ungár T, Zsoldos L, Tichy G. Nature 2004;428:837–40.
[6] Cordier P, Amodeo J, Carrez P. Nature 2012;481:177–80.
[7] Matsunaga T, Saka H. Philos Mag Lett 2000;80:597–604.

[8] Zhang Z, Sigle W, Kurtz W, Rühle M. Phys Rev B 2002;66:214112.

[9] Castillo Rodríguez M, Sigle W. Scripta Mater 2010;62:270–3.

[10] Hirel P, Marton P, Mrovec M, Elsässer C. Acta Mater 2010;58:6072–9.

[11] Lin M-H, Lu H-Y. Mater Sci Eng A 2002;333:41–4.

[12] Wang Y, Poirier J-P, Liebermann R. Phys Chem Miner 1989;16:630–3.

[13] Besson P, Poirier J, Price G. Phys Chem Miner 1996;23:337–44.

[14] Ferré D, Carrez P, Cordier P. Phys Chem Miner 2009;36:233–9.

[15] Miyagi L, Merkel S, Yagi T, Sata N, Ohishi Y, Wenk H-R. Phys Earth Planet Inter 2009;174:159–64.

[16] Ferré D, Cordier P, Carrez P. Am Mineral 2009;94:135–42.

[17] Mainprice D, Tommasi A, Ferré D, Carrez P, Cordier P. Sci Lett 2008;271:135–44.

[18] Shim S-H, Duffy T, Jeanloz R, Shen G. Geophys Res Lett 2004;31:L10603.

[19] Murakami M, Hirose K, Kawamura K, Sata N, Ohishi Y. Science 2004;304:855–8.

[20] Oganov A, Ono S. Nature 2004;430:445–8.

[21] Yagi T, Mao H-K, Bell P. Phys Chem Miner 1978;3:97–110.

[22] Fiquet G, Dewaele A, Andrault D, Kunz M, Le Bihan T. Geophys Res Lett 2000;27:21–4.

[23] Plimpton S. J Comput Phys 1995;117:1–19. <http://lammps.sandia.gov> .

[24] Oganov A, Brodholt J, Price G. Phys Earth Planet Inter 2000;122:277–88.

[25] Gouriet K, Carrez P, Cordier P. Modell Simul Mater Sci Eng 2014;22:025020.

[26] Vitek V. Philos Mag 1968;18:773–86.

[27] Bulatov VV, Cai W. Computer simulations of dislocations. Oxford: Oxford University Press; 2006.

[28] Peierls R. Proc Phys Soc 1940;52:34–7.

[29] Wu X, Vanderbilt D, Hamann D. Phys Rev B 2005;72:035105.

[30] Gumbsch P, Taeri Baghbadrani S, Brunner D, Sigle W, Rühle M. Phys Rev Lett 2001;87:085505.

[31] Brunner D, Taeri Baghbadrani S, Sigle W, Rühle M. J Am Ceram Soc 2001;84:1161–3.

[32] Hirth J, Lothe J. Theory of dislocations. 2nd ed. New York: McGraw-Hill; 1982.

[33] Alfredsson M, Brodholt J, Dobson D, Oganov A, Catlow C, Parker S, et al. Phys Chem Miner 2005;31:671–82.

[34] Chen Q, Cheng X-I, Yang X-D. Chin J Chem Phys 2007;20:547–51.

[35] Ren Q, Joós B, Duesbery M. Phys Rev B 1995;52:13223–8.

[36] Bulatov V, Kaxiras E. Phys Rev Lett 1997;78:4221–4.

[37] Schoeck G. Acta Mater 2006;54:4865–70.

[38] Wang Z, Karato S-I, Fujino K. Phys Earth Planet Inter 1993;79:299–312.

[39] Doukhan N, Doukhan J. Phys Chem Miner 1986;13:403–10.

[40] Beauchesne S, Poirier J. Phys Earth Planet Inter 1989;55:187–99.

[41] Wright K, Price G, Poirier J-P. Phys Earth Planet Inter 1992;74:9–22.

[42] Wang Z-C, Dupas Bruzek C, Karato S. Phys Earth Planet Inter 1999;110:51–69.

[43] Beauchesne S, Poirier J. Phys Earth Planet Inter 1990;61:182–98.

[44] Hirel P, Mrovec M, Elsässer C. Acta Mater 2012;60:329–38.